Finite-Frequency Topological Maxwell Modes in Mechanical Self-Dual Kagome Lattices

Hrishikesh Danawe,[1] Heqiu Li,[2,3] Kai Sun,[2] and Serife Tol[1]
[1]Department of Mechanical Engineering, University of Michigan, Ann Arbor, Michigan 48109-2125, USA
[2]Department of Physics, University of Michigan, Ann Arbor, Michigan 48109-2125, USA
[3]Department of Physics, University of Toronto, Toronto, Ontario M5S 1A7, Canada

(Received 2 May 2022; accepted 12 October 2022; published 10 November 2022)

In this Letter, an elastic twisted kagome lattice at a critical twist angle, called self-dual kagome lattice, is shown to exhibit peculiar finite-frequency topological modes which emerge when certain conditions are satisfied. These states are topologically reminiscent of the zero energy (floppy) modes of Maxwell lattices, but they occur at a finite frequency in the band gap of the self-dual kagome lattice. Thus, we present a completely new class of topological modes that share similarities with both the zero frequency floppy modes in Maxwell lattices and the finite energy in-gap modes in topological insulators. We envision the presented mathematical and numerical framework to be invaluable for many technological advances pertaining to wave phenomena, such as reconfigurable waveguide designs.

DOI: 10.1103/PhysRevLett.129.204302

Introduction.—In the past few years, the concept of topological mechanical or elastic systems [1–18] and other bosonic systems [19–22] have led to a variety of intriguing development. In analogy to topological states in quantum many-body systems, the nontrivial topology structure from phonon bands grants these materials novel properties such as topologically protected edge, surface or corner modes. In general, current studies about topological mechanical or elastic systems can be classified into two categories. In the first category, the dynamic matrix of an elastic system is mapped to the Hamiltonian of an electronic system. Utilizing topological classifications developed for electronic systems [23–28], this mapping enables mechanical systems to achieve the same type of topological phenomena, such as topological edge states in quantum Hall (or spin-Hall or valley-Hall) insulators [3–6,10–15,17]. The second category is known as Maxwell systems [1,2,8,9,16]. For these systems, the nontrivial topology is not coded in the dynamic matrix. Instead, it focuses on the connection between elastic constraints and the degrees of freedom, which maps the elastic problem into a superconductor known as the BDI class [1,25,26]. From there, topological indices can be defined, which govern zero-energy topological states at edges.

These two classes of topological mechanical systems involve totally different concepts and theoretical descriptions. More importantly, they exhibit distinct topological phenomena. For topological systems in the first category, the topological phenomenon has to manifest itself as high-frequency physics, i.e., the topological edge, surface or corner states can only arise between two phonon bands (above the acoustic bands), and fundamental physics principles prevent such topological states from emerging below the acoustic band. This is because the acoustic band is the lowest phonon band, and thus if mapped to electrons, topological indices are required to be zero below the lowest available energy bands. For the second category, on the contrary, topological states must be at (or close to) zero energy, which is below the lowest phonon bands, and fundamental physics principles prohibit such topological states from arising above the acoustic band. In other words, these two classes of topological phenomena are separated in frequency by fundamental principles. There is also an important difference between these two categories regarding the dispersion of edge modes. In the first category, topological edge modes are typically disperse (usually connect the bulk bands above and below the gap). In contrast, topological edge modes in Maxwell systems are dispersionless (i.e., they form flat bands).

Very recently, a new phenomenon was discovered in the elastic lattices called mechanical duality, where the mechanics of two apparently different physical systems is related via mathematical mappings. If the system maps onto itself, then it is called self-dual, and it shows remarkable properties. Recently, Fruchart *et al.* [29] found that the elastic twisted kagome lattices show duality while transitioning through their collapse mechanism [30] where two different structural configurations, equidistant from a mechanical critical point, have the same dynamic characteristics and related elastic moduli. At the critical point, the twisted kagome lattice is self-dual and has a two-fold degenerate dispersion band structure. Later, Gonella [31] numerically demonstrated the duality in twisted kagome lattices by stitching together two dual configurations forming a heterogeneous bidomain structure. More recently, Danawe *et al.* [18] observed peculiar $(d-2)$-dimensional in-gap corner modes in a self-dual kagome lattice occurring at a finite in-gap frequency.

In this Letter, we show that with the help of mechanical duality, a new type of topological mechanical system arises, which exhibits properties of both categories discussed above. Same as the first category, these topological states arise at a high frequency above acoustic bands, in band gaps between various phonon bands. However, the origin and topological structure of these topological states follow the same principle as Maxwell systems, and the topological edge (or domain-wall) states are dispersionless. We demonstrate this new topological phenomenon in the self-dual kagome lattice which satisfies the Maxwell condition relating the degrees of freedom and applied constraints. However, the finite frequency topological Maxwell modes may also be observed in other self-dual lattices.

Self-dual kagome lattice.—A kagome lattice is characterized by three equal masses m located at lattice sites A, B, and C on the vertices of an equilateral triangle, as shown in Fig. 1(a). The masses are interconnected by elastic bonds of stiffness k. In the self-dual kagome lattice, the neighboring bonds connecting same types of lattice sites are perpendicular to each other. For example, in Fig. 1(a), the two CA bonds are at 90° to each other, and similarly, the two CB bonds and two AB bonds are perpendicular to each other as well. The mass at each node can translate in the x and y directions, and the displacement of the ℓth node can be represented by a 2D vector $\mathbf{u}_\ell^T = (u_\ell^x, u_\ell^y)$, i.e., two degrees of freedom per node. By virtue of the periodicity, the displacements of nodes 2–4 and 3–5 are related and governed by Bloch's theorem, such that

$$\mathbf{u}_4 = e^{i\mathbf{k}\cdot\mathbf{e}_1}\mathbf{u}_2 = e^{iq_1}\mathbf{u}_2 \tag{1a}$$

$$\mathbf{u}_5 = e^{i\mathbf{k}\cdot\mathbf{e}_2}\mathbf{u}_3 = e^{iq_2}\mathbf{u}_3 \tag{1b}$$

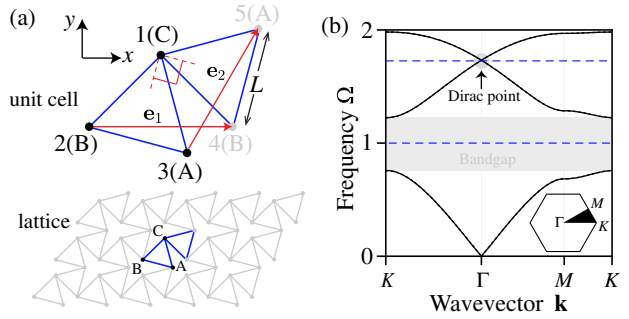

FIG. 1. (a) A self-dual twisted kagome lattice and its unit cell with three equal masses at lattice sites A, B, and C interconnected by bonds of stiffness k, $\mathbf{e}_1$ and $\mathbf{e}_2$ are the direct lattice basis vectors. (b) The dispersion band structure of a self-dual kagome lattice with all free lattice sites (solid lines) and pinned C lattice sites (dotted lines). The flat bands for a lattice with pinned C sites appear at $\Omega = 1$ (in the band gap of free lattice) and $\Omega = \sqrt{3}$ (at Dirac point of free lattice), where $\Omega = \omega\sqrt{(m/k)}$. The first irreducible Brillouin zone K-Γ-M-K is shown in the inset.

where $\mathbf{k}$ is the Bloch wave vector, $\mathbf{e}_1$, $\mathbf{e}_2$ are direct lattice basis vectors such that $|\mathbf{e}_1| = |\mathbf{e}_2| = \sqrt{2}L$ (L is the bond length) and q_1, q_2 are reduced (normalized) wave vectors given by $q_1 = \mathbf{k}\cdot\mathbf{e}_1$, $q_2 = \mathbf{k}\cdot\mathbf{e}_2$. Thus there are a total of six degrees of freedom (DOF) per unit cell corresponding to the three nodes 1, 2, and 3. The dispersion band structure of a self-dual kagome lattice is shown in Fig. 1(b), having three doubly degenerate dispersion branches (solid lines), i.e., for every wave vector $\mathbf{k}$ there are three pairs of identical eigenfrequencies. Now, if the C sites of the lattice are pinned, the unit cell is left with only four DOF, and the band structure reduces to two doubly degenerate flat bands, as shown by dotted lines in Fig. 1(b) (see Supplemental Material for more details [32]). Interestingly, the flat bands at $\Omega = 1$ (where Ω is normalized frequency given as $\Omega = \omega\sqrt{(m/k)}$) are in the band gap of the lattice with all free sites and that at $\Omega = \sqrt{3}$ passes through the Dirac point of the free lattice band structure. For more details on the band structure calculation of a twisted kagome lattice as a function of the twist angle, see Ref. [18], where the author demonstrated the existence of corner modes in a self-dual kagome lattice which also evidently happen to appear at $\Omega = 1$ characterized by zero deformation of the same type of lattice sites as if they are pinned. In this Letter, we further investigate the localized states near intentionally pinned sites of the same type (A, B, or C) in the bulk of a self-dual kagome lattice lattice, seeking the reason for their existence and topological nature.

Finite-frequency localized modes.—What will happen if some (but not all) of the C sites are pinned? For such a partially pinned self-dual kagome lattice, it turns out that an intriguing phenomenon emerges: no matter how many C sites we choose and regardless of which C sites are selected, each pinned C site always generates four modes localized around this site, two at frequency $\Omega = 1$ and two at $\Omega = \sqrt{3}$ (see Supplemental Material for more details [32]). In a lattice system, localized modes induced by a pinned site are not uncommon. However, if we pin two (or more) sites close to each other, these localized modes will typically hybridize with each other, and thus their frequency shall shift depending on the distance between these pinned sites. Such hybridization never arises in the self-dual kagome lattice, and the frequencies of these localized modes always remain exact $\Omega = 1$ or $\sqrt{3}$, even if two pinned C sites are right next to each other. This absence of hybridization is a unique property of this self-dual lattice and is one of the key results of this study. The lack of hybridization results from the unique displacement fields that characterize these modes (see section *Topology and analytic theory* for more details).

In addition, these localized modes also have some other intriguing properties. First, although only some of the C sites are pinned, for all these $\Omega = 1$ or $\sqrt{3}$ modes, all C sites in the entire lattice exhibit zero displacement

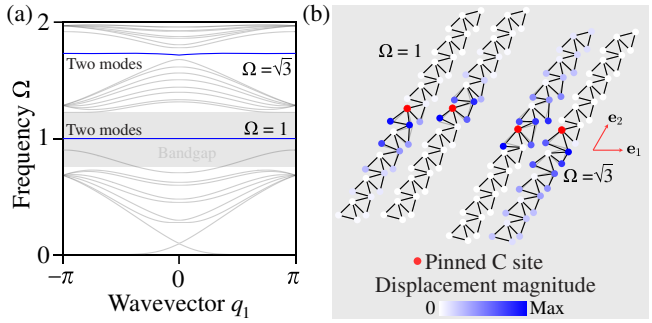

FIG. 2. (a) Eigenfrequencies of a supercell with a pinned lattice site in the bulk. The two doubly degenerate flat bands appear at $\Omega = 1$ and $\Omega = \sqrt{3}$. (b) The mode shapes corresponding to the flat bands at $\Omega = 1$ and $\Omega = \sqrt{3}$ localized near the pinned lattice site for $q_1 = 2\pi/10$. The two modes, at the same frequency, decay away from the pinned lattice site in opposite directions with the same decay rate.

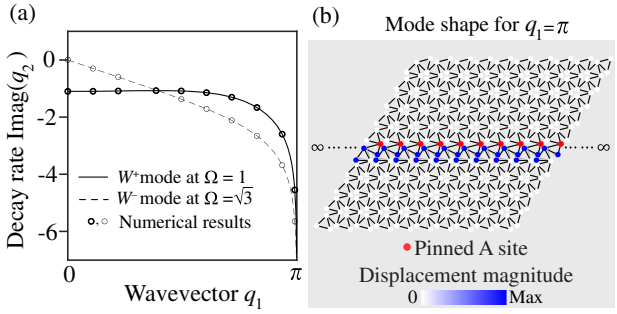

FIG. 3. (a) The decay rate of edge modes obtained from the compatibility matrix formulation compared with the decay rate from supercell simulations. (b) The mode shape of a infinite ribbon with pinned row of A lattice sites for $q_1 = \pi$ at which the decay rates approach $-\infty$ resulting in the highly localized edge mode near the pinned row of lattice sites.

(i.e., all C sites are effectively pinned) similar to the corner modes observed in Ref. [18]. Second, this phenomenon is extremely robust and doesn't exhibit any finite-size or boundary effect. The same phenomenon and exact frequencies are observed regardless of system size (from a few unit cells to infinite lattices) or boundary conditions (open or periodic). The location of the pinned sites (near the edge or in the bulk) has no impact either.

Because these localized modes never hybridize with each other, we can use them as the building blocks to create more complicated structures. For example, if we pin one row of C sites along a straight or zigzag line, these localized modes will form a 1D waveguide, with four 1D flat bands, two at $\Omega = 1$ and two at $\Omega = \sqrt{3}$. If two rows of C sites are pinned, two such waveguides are obtained. Even if the two waveguides are very close to each other, the waveguide modes will not hybridize between the two waveguides. If we pin all the C sites, these localized modes produce four 2D flat bands, as shown in Fig. 1(b). To better demonstrate this effect, in Fig. 2(a), we present the phonon band structure with one row of C sites pinned down, calculated using the supercell shown in Fig. 2(b). Two flat 1D bands at $\Omega = 1$ and two at $\Omega = \sqrt{3}$ are obtained. These modes are localized near the row of pinned C sites (except at $q_1 = 0$, $\Omega = \sqrt{3}$) with exponentially decaying mode shapes away from the pinned sites, as shown in Fig. 2(b). Note that the slightly nonflat shape of the flat bands at $\Omega = \sqrt{3}$ is due to the finite size of the supercell and very low decay rate near $q_1 = 0$ [see Fig. 3(a)]. The edge modes at $\Omega = \sqrt{3}$ and $q_1 = 0$ coexist with bulk modes corresponding to the Dirac point [see Fig. 1(b)].

Topology and analytic theory.—It turns out that these robust features have the same topological origin as the zero-frequency topological edge modes in Maxwell systems, i.e., a topological winding number from the Maxwell counting argument [1,2,8]. However, because the topological modes here are at finite frequencies, a new type of localized basis needs to be introduced.

In a lattice system, any deformation can be characterized by the displacement field $\mathbf{W} = (\mathbf{u}_1^T, \mathbf{u}_2^T, \ldots, \mathbf{u}_{N_s}^T)^T$, where $\mathbf{u}_i$ is the deformation vector of the ith lattice site. This deformation vector has $d \times N_s$ components, where d is the space dimension, and N_s is the number of sites. We define two special sets of deformation fields, $\mathbf{W}^+_{\langle i,j\rangle}$ and $\mathbf{W}^-_{\langle i,j\rangle}$, which will serve as a basis of our topological modes. Here, $\langle i, j\rangle$ represents a bond connecting two neighboring sites i and j. For the deformation $\mathbf{W}^+_{\langle i,j\rangle}$, all other lattice sites exhibit zero displacement, except sites i and j, which share the same displacement vector, $\mathbf{u}_i = \mathbf{u}_j = \mathbf{n}_{\langle i,j\rangle}$ with $\mathbf{n}_{i,j}$ is the unit vector along the bond $\langle i, j\rangle$. For $\mathbf{W}^-_{\langle i,j\rangle}$, it is very similar except that i and j have opposite displacements $\mathbf{u}_i = -\mathbf{u}_j = \mathbf{n}_{\langle i,j\rangle}$.

Here, we focus on symmetric deformations $\mathbf{W}^+$, which give eigenmodes at $\Omega = 1$. The antisymmetric ones $\mathbf{W}^-$ follow exactly the same physics, and they produce eigenmodes at $\Omega = \sqrt{3}$. Using symmetric deformations $\mathbf{W}^+$, we can construct the following displacement field:

$$\mathbf{W}_{AB} = \sum_{\langle A_i,B_j\rangle} \mathcal{A}_{\langle A_i,B_j\rangle} \mathbf{W}^+_{\langle A_i,B_j\rangle}. \tag{2}$$

This deformation is a linear superposition of $\mathbf{W}^+$, and $\mathcal{A}_{\langle A_i,B_j\rangle}$ is the amplitude for each $\mathbf{W}^+$. Here, we only use bonds connecting an A site and a B site, and therefore all C sites have zero deformation. Similarly, we can define $\mathbf{W}_{CA}$ or $\mathbf{W}_{BC}$ using CA or BC bonds, respectively. Here, we shall focus on $\mathbf{W}_{AB}$, and the same results can be easily generalized to $\mathbf{W}_{CA}$ and $\mathbf{W}_{CB}$.

In general, $\mathbf{W}_{AB}$ is not an eigenmode of the dynamic matrix. However, it is straightforward to verify that for the self-dual lattice, $\mathbf{W}_{AB}$ becomes an eigenmode with frequency $\Omega = 1$ if the following constraint is obeyed: all C

sites stay at their equilibrium positions (pinned or at force balance). Therefore, to study the $\Omega = 1$ modes, we can use the linear space of $\mathbf{W}_{AB}$, where the number of degrees of freedom is the number of AB bonds $N_{\mathrm{DOF}} = N_{AB}$. At the same time, without pinning, the total number of constraints is $N_c = 2N_C$, because the x and y components of the total force on each C site need to remain zero. Remarkably, for a kagome lattice, these two numbers coincide, $N_{\mathrm{DOF}} = N_c$, and thus the system is at the Maxwell point.

Same as in topological mechanics, here we can define an effective compatibility matrix to connect the degrees of freedom and the constraints.

$$\mathbf{F} = \mathbf{C}_{\mathbf{eff}}\mathcal{A} \tag{3}$$

Here, $\mathbf{F} = (F_{1,x}, F_{1,y}, F_{2,x}, F_{2,x}\ldots)^T$ is a N_c component vector, where $F_{i,x}$ and $F_{i,y}$ are the x and y components of the total force on the ith C site. $\mathcal{A}$ is a N_{DOF} dimensional vector composed of the coefficients $\mathcal{A}$ in Eq. (2).

In analogy to Maxwell topological mechanics, the null space of the $\mathbf{C}_{\mathbf{eff}}$ matrix (i.e., all modes obeying $\mathbf{C}_{\mathbf{eff}}\mathcal{A} = 0$) corresponds to $\mathbf{W}^+$ modes at $\Omega = 1$. For a lattice with periodic boundary conditions and without any pinning sites, $N_c = N_{\mathrm{DOF}}$, and thus $\mathbf{C}_{\mathbf{eff}}$ is a square matrix. As shown in the Supplemental Material [32], here $\det \mathbf{C}_{\mathbf{eff}} \neq 0$, and thus the null space is empty, indicating the absence of any $\Omega = 1$ modes. However, once some C sites are pinned, $\mathbf{C}_{\mathbf{eff}}$ is no longer a square matrix. Instead, the number of degrees of freedom now exceeds the number of constraints $N_{\mathrm{DOF}} > N_c$, and thus the null space shall contain $N_{\mathrm{DOF}} - N_c$ independent modes. It is easy to realize that for every pinned C site, N_c reduces by 2 and thus $N_{\mathrm{DOF}} - N_c$ increases by 2. This is the reason why we obtained two $\Omega = 1$ modes for every pinned C site. The same approach and conclusions also apply to $\mathbf{W}^-$ modes at $\Omega = \sqrt{3}$, except that we have bulk $\mathbf{W}^-$ modes at the zero wave vector corresponding to the Dirac point.

Same as in Maxwell topological mechanics, a topological index can be defined for this $\mathbf{C}_{\mathbf{eff}}$ matrix, which dictates the number of topologically protected edge or domain-wall modes [1,2,8,16]. To define this index, we need to switch to the momentum space, where the $\mathbf{C}_{\mathbf{eff}}$ becomes (see Supplemental Material [32])

$$\mathbf{C}_{\mathbf{eff}} = k\begin{pmatrix} \frac{1}{2} + \frac{3}{4}(e^{iq_1} + e^{iq_2}) & \frac{\sqrt{3}}{4}(e^{-iq_1} - e^{-iq_2}) \\ -\frac{\sqrt{3}}{4}(e^{iq_1} - e^{iq_2}) & \frac{1}{2} + \frac{3}{4}(e^{-iq_1} + e^{-iq_2}) \end{pmatrix}. \tag{4}$$

For each value of q_1, a topological winding number can be defined as

$$n = \oint \frac{dz}{2\pi i}\mathrm{tr}(\mathbf{C}_{\mathbf{eff}}^{-1}\partial_z \mathbf{C}_{\mathbf{eff}}) \tag{5}$$

where $z = e^{iq_2}$. Using the gauge-invariant integral contour introduced in Ref. [16], (i.e., the unit circle on the complex z plane and remove the residue at $z = 0$ or $z = \infty$), we can obtain two integer topological indices. For a line of pinned C sites (Fig. 2), at each q_1, these two topological indices dictate the number of topologically protected modes localized above and below the pinned line, respectively (i.e., with a negative or positive decay rate). For the $\mathbf{C}_{\mathbf{eff}}$ matrix here, both of the two indices are unity, which means that for each q_1, we have two modes at $\Omega = 1$ localized near this 1D line, one above and one below, in full agreement with numerical simulations.

In addition to the number of modes, the $\mathbf{C}_{\mathbf{eff}}$ matrix also dictates their localization length and mode shape, the same as Maxwell zero mode [1,2,7,8,16,33]. For a given q_1, the equation $\det \mathbf{C}_{\mathbf{eff}} = 0$ has a complex q_2 solution, and its imaginary part is the decay rate

$$\mathrm{Im}q_2 = \ln\left(\frac{14 + 6\cos q_1 - \sqrt{142 + 96\cos q_1 + 18\cos 2q_1}}{12\cos\frac{q_1}{2}}\right). \tag{6}$$

As shown in Fig. 3(a), this analytic prediction perfectly agrees with the decay rates measured from supercell simulations.

Loosely pinned waveguides.—Instead of complete pinning, loosely pinning the lattice sites using an elastic foundation of finite spring stiffness (here $4k$) results in eigenfrequency solutions of a supercell as depicted in Fig. 4(a). The flat bands appearing in the band gap of a supercell with pinned lattice sites [Fig. 2(a)] are not flat in the case of a supercell with loosely pinned sites; however, they are still twofold degenerate. The nonzero

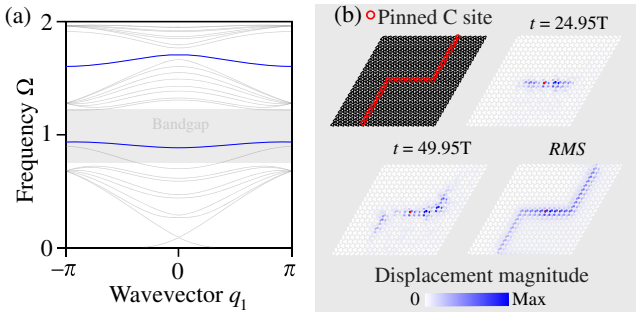

FIG. 4. (a) Eigenfrequencies of a supercell with a loosely pinned lattice site. The flat bands of the supercell with pinned lattice site become dispersive due to loose pinning, but they remain twofold degenerate. (b) Wave propagation along the loosely pinned C sites in a finite lattice due to nonzero group velocity. The unit cell at the middle of the zigzag waveguide with a pinned lattice site is excited using a harmonic excitation and the displacement field is obtained as a function of time. The time snapshots are taken at different instances indicated in terms of time period, T, of harmonic oscillation.

group velocity allows transmission of wave energy along the row of loosely pinned lattice sites, whereas the bulk of the lattice remains isolated due to the band gap. We demonstrate this selective wave propagation in a finite lattice by loosely pinning lattice sites forming a zigzag shape waveguide, as shown in Fig. 4(b). The time snapshots and root mean square (rms) of the displacement field show that the disturbance at the middle of the zigzag-shaped waveguide travels symmetrically in either direction along the row of loosely pinned lattice sites (see Supplemental Material for animations [32]). The loosely pinned waveguide is reconfigurable by simply pinning and unpinning lattice sites, which is not so trivial in the case of quantum spin-Hall or valley Hall systems. Moreover, by controlling the pinning stiffness, the wave speed along the loosely pinned waveguide can be tuned for faster or slower transmission. Note that, unlike quantum Hall systems, the wave propagation along the loosely pinned waveguide is not unidirectional and thus does not offer protection against backscattering. However, the new topological phenomenon avoids unwanted hybridization (interference) between two neighboring waveguides and offers reconfigurability and tunability of waveguides which may have a significant impact on wave propagation applications.

Previously, duality in kagome lattices was experimentally demonstrated using LEGO™ bricks [29]. Also, floppy modes of Maxwell lattices were realized in experiments using near-to-ideal hinges [9]. Moreover, 3D printing [34], bistable structures [35], and nanoparticle self-assembly [36] have also been used in previous studies to realize kagome or topological kagome lattices. Thus, in principle, similar setups can be used to experimentally demonstrate the observed topological modes in the current study. Nonetheless, designing a proper experimental setup to validate the present topological phenomenon would be part of our future work, along with exploring non-Hermitian effects [37–39] on these modes.

Conclusions.—In this Letter, we analyzed a new type of topological state in a self-dual kagome lattice, which exists at two specific frequencies $\Omega = 1, \sqrt{3}$ localized near pinned sites of a sublattice. These states appear at the Maxwell point, where the number of degrees of freedom is equal to the number of constraints. Although analogous to topological mechanics in Maxwell lattices, the Maxwell relation obtained for the self-dual kagome lattice is fundamentally different, and the modes are at finite frequency instead of zero frequency floppy modes, but they retain their dispersionless (flat band) behavior. These modes exhibit special deformation fields, which are characterized by equal deformation of two lattice sites along the bond connecting them while the deformation of the rest of the sites is zero. For a row of pinned sites of a sublattice, the topological modes are localized near the pinned sites while decaying exponentially in bulk. The decay rate is obtained from the determinant of the effective compatibility matrix, and it is compared with supercell simulations with excellent agreement. The topological index for these modes is the same as that for zero-frequency modes in Maxwell lattices, and it corroborates the existence of two topological modes at frequencies $\Omega = 1$ and $\sqrt{3}$.

This work was supported in part by the National Science Foundation, Grant No. CMMI-1914583 (H. D. and S. T.) and the Office of Naval Research MURI N00014-20-1-2479 (H. L. and K. S.).

[1] C. L. Kane and T. C. Lubensky, Topological boundary modes in isostatic lattices, Nat. Phys. **10**, 39 (2014).
[2] T. Lubensky, C. Kane, X. Mao, A. Souslov, and K. Sun, Phonons and elasticity in critically coordinated lattices, Rep. Prog. Phys. **78**, 073901 (2015).
[3] P. Wang, L. Lu, and K. Bertoldi, Topological Phononic Crystals with One-Way Elastic Edge Waves, Phys. Rev. Lett. **115**, 104302 (2015).
[4] A. B. Khanikaev, R. Fleury, S. H. Mousavi, and A. Alù, Topologically robust sound propagation in an angular-momentum-biased graphene-like resonator lattice, Nat. Commun. **6**, 8260 (2015).
[5] C. He, X. Ni, H. Ge, X.-C. C. Sun, Y.-B. B. F. Y.-F. Chen, M.-H. H. Lu, X.-P. P. Liu, and Y.-B. B. F. Y.-F. Chen, Acoustic topological insulator and robust one-way sound transport, Nat. Phys. **12**, 1124 (2016).
[6] X. Ni, M. A. Gorlach, A. Alu, and A. B. Khanikaev, Topological edge states in acoustic kagome lattices, New J. Phys. **19**, 055002 (2017).
[7] D. Rocklin, S. Zhou, K. Sun, and X. Mao, Transformable topological mechanical metamaterials, Nat. Commun. **8**, 14201 (2017).
[8] X. Mao and T. C. Lubensky, Maxwell lattices and topological mechanics, Annu. Rev. Condens. Matter Phys. **9**, 413 (2018).
[9] J. Ma, D. Zhou, K. Sun, X. Mao, and S. Gonella, Edge Modes and Asymmetric Wave Transport in Topological Lattices: Experimental Characterization at Finite Frequencies, Phys. Rev. Lett. **121**, 094301 (2018).
[10] H. Chen, H. Nassar, and G. L. Huang, A study of topological effects in 1D and 2D mechanical lattices, J. Mech. Phys. Solids **117**, 22 (2018).
[11] H. Chen, H. Nassar, A. N. Norris, G. K. Hu, and G. L. Huang, Elastic quantum spin Hall effect in kagome lattices, Phys. Rev. B **98**, 094302 (2018).
[12] G. Ma, M. Xiao, and C. T. Chan, Topological phases in acoustic and mechanical systems, Nat. Rev. Phys. **1**, 281 (2019).
[13] J. Ma, K. Sun, and S. Gonella, Valley Hall In-Plane Edge States as Building Blocks for Elastodynamic Logic Circuits, Phys. Rev. Appl. **12**, 044015 (2019).
[14] T. W. Liu and F. Semperlotti, Experimental Evidence of Robust Acoustic Valley Hall Edge States in a Nonresonant Topological Elastic Waveguide, Phys. Rev. Appl. **11**, 014040 (2019).
[15] H. Xue, Y. Yang, F. Gao, Y. Chong, and B. Zhang, Acoustic higher-order topological insulator on a kagome lattice, Nat. Mater. **18**, 108 (2019).

[16] K. Sun and X. Mao, Continuum Theory for Topological Edge Soft Modes, Phys. Rev. Lett. **124**, 207601 (2020).
[17] Q. Wu, H. Chen, X. Li, and G. Huang, In-Plane Second-Order Topologically Protected States in Elastic Kagome Lattices, Phys. Rev. Appl. **14**, 014084 (2020).
[18] H. Danawe, H. Li, H. A. Ba'ba'a, and S. Tol, Existence of corner modes in elastic twisted kagome lattices, Phys. Rev. B **104**, L241107 (2021).
[19] T. Ozawa, H. M. Price, A. Amo, N. Goldman, M. Hafezi, L. Lu, M. C. Rechtsman, D. Schuster, J. Simon, O. Zilberberg, and I. Carusotto, Topological photonics, Rev. Mod. Phys. **91**, 015006 (2019).
[20] V. Peano, C. Brendel, M. Schmidt, and F. Marquardt, Topological Phases of Sound and Light, Phys. Rev. X **5**, 031011 (2015).
[21] H. Ren, M. Matheny, G. MacCabe, R. Luo, H. Pfeifer, M. Mirhosseini, and O. Painter, Two-dimensional optomechanical crystal cavity with high quantum cooperativity, Nat. Commun. **11**, 3373 (2020).
[22] J. P. Mathew, J. D. Pino, and E. Verhagen, Synthetic gauge fields for phonon transport in a nano-optomechanical system, Nat. Nanotechnol. **15**, 198 (2020).
[23] M. Z. Hasan and C. L. Kane, *Colloquium*: Topological insulators, Rev. Mod. Phys. **82**, 3045 (2010).
[24] X.-L. Qi and S.-C. Zhang, Topological insulators and superconductors, Rev. Mod. Phys. **83**, 1057 (2011).
[25] A. Kitaev, Periodic table for topological insulators and superconductors, AIP Conf. Proc. **1134**, 22 (2009).
[26] A. P. Schnyder, S. Ryu, A. Furusaki, and A. W. W. Ludwig, Classification of topological insulators and superconductors in three spatial dimensions, Phys. Rev. B **78**, 195125 (2008).
[27] H. C. Po, A. Vishwanath, and H. Watanabe, Symmetry-based indicators of band topology in the 230 space groups, Nat. Commun. **8**, 50 (2017).
[28] B. Bradlyn, E. L., J. Cano, M. G. Vergniory, Z. Wang, M. I. Felser, C. Aroyo, and B. A. Bernevig, Topological quantum chemistry, Nature (London) **547**, 298 (2017).
[29] M. Fruchart, Y. Zhou, and V. Vitelli, Dualities and non-Abelian mechanics, Nature (London) **577**, 636 (2020).
[30] S. Guest and J. Hutchinson, On the determinacy of repetitive structures, J. Mech. Phys. Solids **51**, 383 (2003).
[31] S. Gonella, Symmetry of the phononic landscape of twisted kagome lattices across the duality boundary, Phys. Rev. B **102**, 140301(R) (2020).
[32] See Supplemental Material at http://link.aps.org/supplemental/10.1103/PhysRevLett.129.204302 for more details on localized states near pinned sites in a finite lattice, dispersion bands of self-dual kagome lattice with pinned sublattice, spatially compact localized states and animation movie of wave transport via loosely pinned waveguides.
[33] K. Sun, A. Souslov, X. Mao, and T. C. Lubensky, Surface phonons, elastic response, and conformal invariance in twisted kagome lattices, Proc. Natl. Acad. Sci. U.S.A. **109**, 12369 (2012).
[34] M. Charara, K. Sun, X. Mao, and S. Gonella, Topological Flexural Modes in Polarized Bilayer Lattices, Phys. Rev. Appl. **16**, 064011 (2021).
[35] H. Xiu, H. Liu, A. Poli, G. Wan, E. M. Arruda, X. Mao, and Z. Chen, Multistable topological mechanical metamaterials, arXiv:2207.05826.
[36] Q. Chen, S. Bae, and S. Granick, Directed self-assembly of a colloidal kagome lattice, Nature (London) **469**, 381 (2011).
[37] E. J. Bergholtz, J. C. Budich, and F. K. Kunst, Exceptional topology of non-Hermitian systems, Rev. Mod. Phys. **93**, 015005 (2021).
[38] A. McDonald, T. Pereg-Barnea, and A. A. Clerk, Phase-Dependent Chiral Transport and Effective Non-Hermitian Dynamics in a Bosonic Kitaev-Majorana Chain, Phys. Rev. X **8**, 041031 (2018).
[39] J. del Pino, J. J. Slim, and E. Verhagen, Non-Hermitian chiral phononics through optomechanically induced squeezing, Nature (London) **606**, 82 (2022).